Published in final edited form as:

Nanomedicine. 2019 January ; 15(1): 129–141. doi:10.1016/j.nano.2018.09.005.

Targeted Codelivery of Doxorubicin and IL-36γ Expression Plasmid for An Optimal Chemo-Gene Combination Therapy against Cancer Lung Metastasis

Yichao Chen[#1], **Jingjing Sun**[#1], **Yixian Huang**[#1], **Yanhua Liu**[2], **Lei Liang**[3], **Da Yang**[1], **Binfeng Lu**[4], and **Song Li**[1]

[1]Center for Pharmacogenetics, Department of Pharmaceutical Sciences, School of Pharmacy, University of Pittsburgh, Pittsburgh, Pennsylvania 15261, USA;

[2]Department of Pharmaceutics, School of Pharmacy, Ningxia Medical University, No. 1160, Shengli Street, Yinchuan 750004, China;

[3]Guangdong Second Provincial General Hospital, Guangzhou, 510317, China;

[4]Department of Immunology, University of Pittsburgh School of Medicine, 200 Lothrop Street, Pittsburgh, PA 15261, USA.

[#] These authors contributed equally to this work.

Abstract

Cancer metastasis is the main cause for the high mortality in breast cancer patients. In this work we developed a polymer POEG-*st*-Pmor for targeted co-delivery of IL-36γ expression plasmid and doxorubicin (Dox) to lung metastasis of breast cancer. The polymer readily formed micelles that were effective in loading Dox and simultaneously forming complexes with IL-36γ plasmid. Interestingly, particles co-loaded with Dox and plasmid was significantly smaller and more stable than the particles loaded with Dox only. Gene transfection in both lungs and s.c. tumors was significantly higher with our polymer compared to PEI. In addition, the Dox+IL-36γ/POEG-*st*-Pmor could not only bring improved anti-metastatic effect but synergistically enhance the type I immune response by increasing the IFN-γ positive $CD4^+$ and $CD8^+$ T cells and simultaneously decreasing the immunosuppressive myeloid-derived suppressor cells in the lung. POEG-*st*-Pmor may represent a simple and effective delivery system for an optimal chemo-gene combination therapy.

Keywords

Cancer metastasis; Co-delivery; DOX; IL-36γ; micelles

Correspondence and requests for materials should be addressed to S.L. (sol4@pitt.edu).

Conflict of interest statement: The authors have declared that no competing interest exists.

Background

Cancer metastasis, which refers to the spread of cancer cells from the primary tumor site to distant tissues or organs, is the main cause of breast cancer-related deaths[1, 2]. Lung, liver, bone and brain are major organs for breast cancer metastases and more than 60% of breast cancer patients show metastasis in lungs at late stages[3, 4]. Although surgery may be effective in treating the primary tumor, chemotherapy is necessary for advanced lung metastases [5, 6]. Despite recent advancements in chemotherapy, the five-year survival rate of metastatic breast cancer remains low (~20%) with serious side effects, mainly due to off-target toxicity[7]. Therefore, the development of therapies to achieve efficient targeting of metastasis is highly demanded, which will likely achieve enhanced therapeutic efficacy and reduced systemic toxicities.

Current lung metastasis targeted delivery largely relies on the size-driven systems such as nanoparticles, micelles and liposomes [8–10]. Although these nanoscale carriers show promising results, drawbacks such as poor stability, complex formulation strategy and potential toxicity remain unresolved[11]. Most current nanocarriers can improve therapeutic effect through enhancement of permeation and retention (EPR) effect in primary tumors with vasculature pore sizes over 100 mm^3 [12]. However, small metastatic tumors are usually less vascularized, which limits the access of nanoparticles to these lesions[13]. Thus, drug delivery systems with well-defined carrier structures, sufficient *in vivo* stability and high targeting efficiency are urgently needed to overcome the current problems. It has been reported that small ligands such as linear tertiary amines on the carriers may benefit lung targeted drug delivery since the lung is proven to be a site for accumulation of numerous basic amines [14, 15]. These studies have inspired us to explore the potential of tertiary amine-derived carriers as targeting systems for treatment of lung metastasis.

We herein developed a multifunctional delivery system that is based on an amphiphilic polymer with morpholine attached to the pendant side chains (POEG-*st*-Pmor) for codelivery of small molecule chemotherapy drugs and plasmid DNA. The hydrophobic anticancer drugs are expected to be incorporated into the hydrophobic core through hydrophobic-hydrophobic interaction and π-π stacking[16]. Morpholine is incorporated into the polymer to introduce positives charges to form complexes with nucleic acids[17]. The positively charged morpholine groups in the polymers can also facilitate the accumulation of the carrier in the lung due to the interaction of positively charged tertiary amine with negatively charged cell membrane in the lung[18, 19]. Doxorubicin (Dox) and IL-36γ plasmid were selected as the model drug and DNA for the combination therapy. Dox is a first-line chemotherapeutic drug in the treatment of a broad range of cancers including breast, ovary, bladder, and lung cancers, and breast cancer metastasis[20, 21]. Cytokines are reported to have a synergistic antitumor effect in combination with conventional antitumor treatments such as chemotherapy[22, 23]. Interleukin 36 (α, β, γ) belongs to IL-1 family of cytokines and the three isoforms share the same receptor complex[24]. IL-36γ is reported to promote the differentiation of type 1 effector lymphocytes, including $CD8^+$, NK, and γδT cells *in vitro*[24, 25]. The tumoral expression of IL-36γ exerts strong antitumor immune responses *in vivo* and transforms the tumor microenvironment in favor of tumor eradication[24]. We hypothesized that codelivery of Dox and IL-36γ plasmid via our

multifunctional carrier represents a simple and effective approach for the treatment of lung metastasis. We first examined the biophysical properties of the nanocarrier co-loaded with Dox and IL-36γ plasmid. The efficiency of delivery and transfection was then examined both *in vitro* and *in vivo*. Finally, the antitumor effect of Dox^+ IL-36γ plasmid/polymer as well as the underlying mechanism was investigated.

Method

Materials and Reagents

Doxorubicin (>99%) was purchased from LC Laboratories (MA, USA). Dicyclohexylcarbodiimide (DCC) was purchased from Alfa Aesar (MA, USA). 4-(Dimethylamino) pyridine (DMAP) was purchased from Calbiochem-Novabiochem Corporation (CA, USA). Vinylbenzyl chloride, 4-Cyano-4-(phenylcarbonothioylthio)pentanoic acid, oligo(ethylene glycol) methacry-late OEGMA (average Mn = 500), 2,2-Azobis(isobutyronitrile) (AIBN), trypsin-EDTA solution, 3-(4,5-dimethylthiazol-2-yl)-2,5-di phenyl tetrazolium bromide (MTT) and Dulbecco's Modified Eagle's Medium (DMEM) were all purchased from Sigma-Aldrich (MO, U.S.A.). Opti-MEM medium was purchased from Invitrogen (Carlsbad, USA). AIBN was purified by recrystallization in anhydrous ethanol. Fetal bovine serum (FBS) and penicillin-streptomycin solution were purchased from Invitrogen (NY, U.S.A.).

Synthesis of VBMor monomer

Vinylbenzyl chloride (167.2 mg, 1.1 mM), morpholine (95.8 mg, 1.1 mM) and K_2CO_3 (0.69 g, 5 mM) were dissolved in 6 mL DMF and stirred at 50°C for 6 h. After cooling down to room temperature, 20 mL water was added to the mixture, followed by three times extraction with 50 mL CH_2Cl_2. After evaporation of CH_2Cl_2, the crude product was purified by column chromatography with petroleum ether/ethyl acetate (v/v, 4/1~2/1) as the elution liquid. VBMor monomer was obtained with a 71% yield.

Synthesis of POEG-st-Pmor polymer

VBMor monomer (228.8 mg, 1.13 mmol), OEG500 (100 mg, 0.20 mmol), AIBN (1 mg, 0.0062 mmol), 4-Cyano-4-(phenylcarbonothioylthio)pentanoic acid (4 mg, 0.014 mmol), and 1 mL of dried tetrahydrofuran were added into a Schlenk tube, and deoxygenated by free-pump-thawing for three times. Then the mixture was filled with N_2 and immersed into an oil bath thermostated at 80 °C to start the polymerization. After 24 h, the reaction was quenched by immersing the tube into liquid nitrogen and the mixture was precipitated in hexane for 3 times. The product POEG-*st*-Pmor was obtained after vacuum drying.

Preparation and characterization of IL-36γ Plasmid/Dox-co-formulated micelles

Dox-loaded POEG-*st*-Pmor micelles were prepared by the dialysis method[26]. Briefly, 10 mg of polymer was dissolved in 5 mL of DMSO and mixed with 100 μL of Dox DMSO solution (10 mg/ml). To remove free Dox from the Dox-incorporated micelles, the solution was dialyzed against PBS using dialysis membrane with a MW cutoff of 3,500. The solution was lyophilized and resolubilized in 1mL PBS. Drug-free micelles were similarly prepared. For plasmid DNA complexation, polymeric micelles were diluted to different concentrations

in water and mixed with plasmid DNA solution to obtain the desired N/P ratios. This mixture was allowed to incubate at RT for 20 min prior to further characterization.

In vitro characterization of polymer

The structure and molecular weight of POEG-st-Pmor polymer was characterized by ^{1}H NMR and gel permeation chromatography (GPC) similarly conducted as previously reported[27]. The particle size and zeta potential of POEG-*st*-Pmor polymer were determined by dynamic light scattering (Nano-ZS 90, Malvern Instruments, Malvern, UK). The morphology of POEG-*st*-Pmor polymers was observed under a transmission electron microscope (TEM). The micelles were placed on a copper grid covered with nitrocellulose. The samples were negatively stained with phosphotungstic acid and dried at room temperature before measurement.

Drug loading capacity (DLC) and drug loading efficiency (DLE) were determined as described before[28, 29]. The amount of Dox loaded in the micelles was determined by high performance liquid chromatography (HPLC, Shimadzu LC-20AD, Japan). The DLC of Dox/micelles was calculated using the equation : DLC=Drug incorporated/(input polymer+Drug) ×100%

Critical micelle concentration

The critical micellar concentration (CMC) was determined using Nile Red as a fluorescence probe[28]. Micelles of various concentrations (0.0001 to 1 mg/mL) were first prepared. Two microliter of a Nile Red solution in acetone (0.97 mg/mL) were then added to each sample and acetone was evaporated prior to fluorescence measurements using a microplate reader. Fluorescence from emission wavelength ranging from 560 to 750nm was recorded with an excitation wavelength of 550 nm.

In vitro drug release study

The *in vitro* Dox release kinetics for the POEG-*st*-Pmor micelles was determined by a dialysis method. Briefly, 0.5ml of Dox-loaded micelles and micelles co-loaded with Dox and IL-36γ plasmid at a Dox concentration of 0.5 mg/mL were placed into a dialysis bag (MW cutoff 3,500), respectively. The dialysis bag was incubated in 100 mL PBS with gentle shaking at 37 °C. Two ml of PBS solution outside of the dialysis bag was collected at different time points and equal amount of fresh PBS was added back. The concentrations of released Dox were determined by HPLC [30].

Gel retardation assay

Plasmid/polymer complexes were prepared at different N/P ratios, ranging from 0.1 to 20 (plasmid DNA concentration was fixed at 5 mg/ml). The resulting complexes were then electrophoresed on a 1% agarose gel in TAE buffer at 120 mV for 30 min, and visualized using a UV illuminator with ethidium bromide staining[31]. Free plasmid DNA was used as a control.

Cell culture and animals

The murine breast cancer cell line 4T1.2 was cultured in DMEM medium supplemented with 10% FBS and 1% penicillin/streptomycin at 37 °C in 5% CO_2 atmosphere. Female BALB/c mice (4–6 weeks, Charles River, Davis, CA) were housed under pathogen-free conditions according to AAALAC guidelines. The mice related experiments were performed following institutional guidelines and approved by the Animal Use and Care Administrative Advisory Committee at the University of Pittsburgh.

In vitro cytotoxicity

The cytotoxicity of Dox-formulated POEG-*st*-Pmor micelles, IL-36γ plasmid-complexed micelles and Dox+IL-36γ plasmid-co-loaded micelles were assessed in 4T1.2 breast cancer cells and compared to free Dox. Briefly, 4T1.2 cells (2,000 cells/well) were seeded in 96-well plates for overnight and were treated with various concentrations of Dox formulations for 72h. MTT solution was added to each well and MTT formazan was solubilized by DMSO after 2h of incubation. The absorbance in each well was measured by a microplate reader at a wavelength of 570 nm[32]. Cell viability was calculated as $[(OD_{treat} - OD_{blank})/(OD_{control} - OD_{blank}) \times 100\%]$. The cytotoxicity of POEG-*st*-Pmor micelles alone was similarly tested in 4T1.2 cells as described above.

Stability of the micelles in BSA

BSA was used to simulate the blood physiological environment to investigate the stability of POEG-*st*-Pmor micelle complexes under the mimicked physiological conditions. Plasmid DNA/micelle complexes and plasmid DNA+Dox/micelle complexes were prepared as described above and incubated with BSA (30 mg/ml). pDNA/PEI complexes were used as a control. Sizes of complexes were followed at different time points as an indication of stability.

In vitro plasmid transfection

4T1.2 cells were seeded in a 96-well plate and incubated for 24 h until cells were 80% confluent. Cells were then transfected with EGFP plasmid/POEG-*st*-Pmor complexes (N/P=20) and EGFP plasmid/PEI (N/P=20) complexes in serum-free opti-DMEM medium. After 4 h incubation, transfection medium was removed and 100 μL of fresh complete medium were added to each well. PBS group was used as a control. After 48h, the transfected cells were observed under a fluorescence microscope (OLYMPUS America, Melville, NY).

In vivo fluorescence imaging

Female Balb/C mice bearing 4T1.2 tumor (~400 mm^3) in the mammary fat pad were used to investigate the biodistribution and *in vivo* transfection efficiency of our micellar carriers.

The *in vivo* transfection efficiency of POEG-*st*-Pmor micellar carriers was evaluated with EGFP plasmid as a reporter gene. Linear PEI was used to as control. Various formulations were i.v. injected into tumor-bearing mice at a dose of 50 μg plasmid per mouse. One day

later, mice were injected with 1 μg of Hoechst and sacrificed one hour later. The fluorescence signal of EGFP in the cryosections was examined under a confocal microscope.

Mouse model of breast cancer lung metastasis

Female Balb/c mice were injected with 2×10^5 4T1.2 cells through the tail vein. Five days after tumor cell injection, mice were randomly divided into 6 groups. POEG-*st*-Pmor was chosen as a representative carrier system for codelivery of IL-36γ plasmid and Dox. Animals were treated intravenously with free POEG-*st*-Pmor micelles, IL-36γ plasmid/POEG-*st*-Pmor micelles, Dox+control plasmid/POEG-*st*-Pmor micelles and Dox+IL-36γ plasmid/POEG-*st*-Pmor micelles every three days for three times. The PBS treatment group was used as control. Dox dosage was 5 mg/kg and plasmid dosage was 50μg per mouse. Lung tissues were harvested and weighted 11 days after the first injection. Pulmonary metastases were enumerated by intra-tracheal injection of India ink solution. India ink-injected lungs were washed in Feket's solution (300 ml 70% EtOH, 30 ml 37% formaldehyde and 5 ml glacial acetic acid) and white tumor nodules against a dark blue lung background were counted.

Histopathological analysis

The lung tissues were harvested and fixed in 10% formalin after the above treatments. The fixed samples were then embedded in paraffin and the tissue sections were stained with hematoxylin/eosin and analyzed for the presence of metastases under microscope. The total number of metastases per lung section was counted in different treatment groups.

Analysis of tumor-infiltrating lymphocytes and myeloid-derived suppressor cells

Lung tissues were collected in serum free RPMI medium and cut mechanically with scissors. Liberase TL (0.3mg/ml) and DNase I (0.3 mg/ml) were used to digest the lung tissues and tumor nodules. Tissues were further grinded and filtered through a 40-mm cell strainer. TILs and MDSC cells were further purified and stained with fluorescence-labeled antibody for flow cytometry analysis using a FACS flow cytometer.

Results

Synthesis of POEG-st-Pmor polymer

The synthesis scheme for POEG-*st*-Pmor polymer was shown in Figure 1A. First, VBMor monomer was synthesized by reacting vinylbenzyl chloride with morpholine. The structure of VBMor monomer was confirmed by ^{1}H NMR as shown in Figure S1 of the Supporting Information. Then, POEG-*st*-Pmor copolymer was prepared via reversible addition-fragmentation chain-transfer (RAFT) polymerization of OEG500 monomer and VBMor monomer. The structures and molecular weight of POEG-*st*-Pmor polymer were characterized by ^{1}H NMR and gel permeation chromatography (GPC). The average degree of polymerization (DP) of the OEG500 monomer was calculated to be 10 according to the conversion of OEG500 monomer at the end of the polymerization (conversation: 70%). The DP of the VBMor monomer was determined to be 60 by comparing the intensities of I_a and I_c (Figure S2 of the Supporting Information). The average molecular weight M_n of POEG-*st*-Pmor polymer determined by GPC is 9260, and the polydispersity is 1.13 (Figure S3),

which indicated the successful synthesis of POEG-*st*-Pmor copolymer with well-defined structure.

Characterization of micellar nanoparticles

POEG-*st*-Pmor micelles were prepared via a dialysis method [26]. As shown in Figure 1B, POEG-*st*-Pmor micelles had sizes around 200 nm as tested with a zetasizer. Spherical structure was observed by TEM. The size tested by TEM is smaller than that by DLS, probably due to the different principles of analysis and the shrinkage of dried micellar nanoparticles during TEM measurement [33–36]. The critical micelle concentration (CMC) of the polymer was determined using nile red as a fluorescence probe. POEG-*st*-Pmor has a low CMC around 0.04 mg/ml (Figure S4).

The Dox-loaded POEG-*st*-Pmor micelles were similarly prepared as blank micelles. POEG-*st*-Pmor carrier could load Dox at a carrier/drug mass ratio starting from 10:1 with sizes ranging from 160 to 190 nm (Figure 1, Table 1) and the formulation could remain stable for two weeks at room temperature. Then we tested whether the POEG-*st*-Pmor could form stable complexes with plasmid DNA. A gel retardation assay was performed to assess the pDNA binding ability of the pMor-based polymer. Plasmid DNA/carrier complexes were fabricated at various N/P ratios from 0.1:1 to 30:1. As shown in Figure 2A, complete complexation of plasmid DNA by POEG-*st*-Pmor polymer was achieved at an N/P ratio of 5/1 or greater. In order to further study the interaction between DNA and carrier, a competitive binding gel-shift assay with dextran sulfate was performed. As shown in Figure 2B, substantial amounts of DNA were released from control PEI/DNA complexes at an S/P ratio (molar ratio between the sulfur from dextran sulfate and the phosphate from pDNA) as low as 15/1. In contrast, no obvious release of DNA was observed for POEG-*st*-Pmor/DNA complexes at an S/P ratio as high as 40/1.

The surface zeta potential of the POEG-*st*-Pmor blank micelles was 26.4 mV before the addition of IL-36γ plasmid (Figure 3A&B and Table 1). At the N/P ratios of below 1, the complexes were negatively charged and the particle sizes were similar to the sizes of the micelles alone. There was a significant increase in the sizes of the complexes at an N/P ratio of 3. At this ratio, the particle charges were close to neutral. Interestingly, further increases in the N/P ratios led to a significant decrease in the particle sizes and the particles became more positively charged with continuous increases in the N/P ratios. Specifically, when the micelles were mixed with IL-36γ plasmid at an N/P ratio of 20:1, the average size of the complexes decreased to 70–80 nm (Table 1, Figure 3A). Nonetheless, DNA/micelle complexes were less positively charged compared to free micelles with a surface zeta potential of 10.3 mV (Table 1).

We then went on to further explore the possibility of co-delivery of pDNA and Dox by POEG-*st*-Pmor micelles. As shown in Figure 1B and Table 1, the size distribution and zeta-potential were not significantly affected when Dox was loaded into the pDNA/polymer complexes at a drug concentration of 1 mg/mL and a carrier/drug ratio of 20/1 (m/m).

Stability of the complexes in BSA

The colloidal stability of micelle/DNA complexes was tested in BSA solution (30mg/mL). PEI/DNA complexes were used as a control (N/P=20, zeta potential=18.3 mV). As shown in Figure 3C, exposure of PEI/DNA complexes to BSA led to a rapid increase in the particle sizes. At 5 h post-incubation, the sizes of PEI/DNA complexes increased from 149 to 261 nm. It is also apparent that POEG-*st*-Pmor/DNA complexes were resistant to BSA-induced aggregation and showed minimal changes in sizes throughout the entire 18 h of observation.

In Vitro Dox Release

The profile of Dox release from the Dox-loaded micelles was examined by a dialysis method with Dox. HCl solution as a control (Figure 3D). Free Dox was rapidly diffused out of the dialysis tubing with 80% of DOX found in the dialysate in the first 4 hours. However, Dox formulated in POEG-*st*-Pmor micelles showed a slow kinetics of release with less than 25% of Dox released outside of dialysis bag at the first 4 hours, and only 35% of Dox released at 24h. The micelles co-loaded with Dox and plasmid exhibited an even slower Dox release profile compared to micelles loaded with Dox alone at later time points. The polymer concentration inside the dialysis bag was far above the CMC value and the micelles were stable throughout the entire course of release study.

In vitro cytotoxicity of blank micelles and Dox+IL36γ plasmid/micelle complexes

The *in vitro* cytotoxicity of Dox+IL36γ plasmid/micelle complexes was evaluated with 4T1.2 breast cancer cells via MTT assay. Cells received various treatments for 72 h and the final concentrations of Dox ranged from 4 to 1000 ng/mL (Figure 4A). The free Dox and the Dox-loaded micelles showed a dose-dependent cell killing profile. The Dox/POEG-*st*-Pmor micelles had lower IC50s (60ng/ml) compared to free Dox (130ng/ml) (Figure 4A). Incorporation of IL36γ plasmid into Dox-loaded micelles led to slightly increased cytotoxicity on 4T1.2 cells. POEG-*st*-Pmor alone showed minimal cytotoxicity to 4T1.2 cells at the polymer concentration as high as 20μg/mL (Figure 4B).

Cellular internalization of nanomicelles

The cellular uptake of Dox-loaded POEG-*st*-Pmor micelles was investigated by confocal laser scanning microscopy with free Dox as a control. As shown in Figure 4C, at 2 h of incubation, Dox-loaded POEG-*st*-Pmor micelles showed more Dox cellular uptake compared to free Dox at the same Dox concentration. The signals for free Dox were largely found in nucleus while the signals for the micellar Dox were mainly located outside the nucleus. This might be due to the different cellular uptake routes of free Dox and Dox micelles.

In vitro and in vivo EGFP transfection

Using EGFP as a reporter gene, we investigated if POEG-*st*-Pmor carrier could effectively deliver EGFP plasmid into 4T1.2 cultured cells and tumor tissues, leading to expression of biologically active protein. Figure 5 shows that 4T1.2 tumor cells were effectively transfected with EGFP plasmid complexed with POEG-*st*-Pmor micelles. 4T1.2 cells were also effectively transfected with branched PEI, a control carrier.

Figure 6 shows the in vivo EGFP expression in tumor, lung and liver tissues. There were significantly more EGFP signals in tumors with POEG-*st*-Pmor formulation compared to linear PEI (Figure 6A). In agreement with previous reports, lungs could be effectively transfected by linear PEI (Figure 6B). However, more and stronger signals of EGFP were observed in lungs transfected with POEG-*st*-Pmor formulation (Figure 6B). Liver was hardly transfected with either our formulation or control linear PEI (Figure 6C). These results suggest that POEG-*st*-Pmor polymer is suitable for *in vivo* gene delivery to both lungs and distant solid tumors.

Anti-tumor activity of micelles co-loaded with Dox and IL-36γ plasmid

A mouse model of breast cancer lung metastasis (4T1.2) was generated in female Balb/c mice and various treatments were given to each group of mice via tail vein injection (Figure 7A). As shown in Figure 7B, the carrier alone did not show therapeutic activity compared to control group. Free Dox showed a significant inhibition of lung metastasis and the antitumor activity was further enhanced for micelles co-loaded with Dox and IL-36γ plasmid compared to free Dox, Dox+control plasmid/micelles and IL-36γ plasmid/micelles. The H&E staining of lung tissues showed clear tumor cell infiltration in all of the groups except the co-delivery group (Figure 7C). The group with more tumor nodules had more lung weights (Figure 7D&E). Body weights were also monitored during the treatment period. No significant decrease of body weight was observed, indicating the safety of the formulation (Figure 7F).

Immune cell infiltration profile in tumor-bearing lungs

Following demonstration of the significant antitumor activity of Dox+IL-36γ plasmid/POEG-*st*-Pmor, we examined the immune cell infiltration in the tumor-bearing lungs to elucidate a role of immune response in the overall antitumor activity. As shown in Figure 8A&C, there was a significant increase of cytotoxic $CD8^+$ T cells in the lung tissues treated with free Dox, IL-36γ plasmid/POEG-*st*-Pmor or the combination of both compared to untreated control group. Although there was no significant difference in the total number of T cells between Dox+IL-36γ plasmid/POEG-*st*-Pmor and Dox+control plasmid/POEG-*st*-Pmor, the numbers of IFN-γ^+ $CD4^+$ and IFN-γ^+ $CD8^+$ T cells were significantly increased in the combination treatment group compared to either of the other treatment groups (Figure 8D–G). We also examined the $CD11^+Gr\text{-}1^+$ immunosuppressive myeloid-derived suppressor cells (MDSCs) in lung tissues. The numbers of MDSCs were significantly decreased in all treatment groups except the carrier alone group (Figure 8H–I). Surprisingly, there was a significant increase in the number of $Foxp3^+$ $CD4^+$ T cells (regulatory T cells (Treg)) in the mice treated with IL-36γ plasmid, alone or in combination with Dox (Figure 8J–K).

Discussion

Most delivery systems developed so far are designed for delivery of either small molecule drugs or nucleic acid-based therapeutics[37, 38]. In this study, we have developed a simple micellar system that is highly effective in codelivery of small molecules and plasmid DNA. Various mechanisms are likely to be involved in the formation of free micelles and drug- or drug/gene-loaded micelles. While the hydrophobic interaction and π-π stacking drive the

formation of a compact particle, the positive charge-mediated repulsion may impose a negative force on the formation of such particle. Loading of DOX into the micelles led to a small decrease in particle sizes (180 vs 160 nm): this is likely due to formation of a more compacted particle, which is facilitated by the carrier-DOX interactions. Interestingly, the particle size was more dramatically reduced following the complexation of the micelles with plasmid DNA in the presence or absence of DOX: the size decreased from 180 nm to about 100 nm. The interaction of large-sized plasmid DNA with the positively charged micelles shall result in a non-covalent cross-linking of micelles. In addition, charge neutralization of DNA is known to induce DNA condensation [39, 40]. Together, these events shall drive the formation of a more compact hydrophobic core and thus significantly decreased particle size. The significantly increased particle size at an N/P ratio of 3/1 is likely due to a status of neutral surface, which drives the aggregation of the nanomicelles. On the other hand, the excess surface positive charges at N/P ratios of above 3/1 help to maintain the colloidal stability of the "condensed" nanomicelles through charge-mediated repulsion. It is interesting to note that one of the issues with nanomicellar formulation is its intrinsic instability [41]. Micelles are formed through the self-assembly of amphiphilic monomers, which is a reversible and dynamic process[42]. Micelles tend to fall apart when they are diluted in the blood upon systemic administration[43, 44]. This can be further aggravated by the lipid exchange as a result of interactions with lipoproteins in the blood[45, 46]. A number of strategies have been reported to cross-link the monomers to stabilize the micelles[47–49]. In our system, the multivalent charge-charge interactions between the cationic polymer and plasmid DNA serve as a simple approach to cross-link the micelles. As a result, micelles that are co-loaded with small molecules and plasmid DNA are likely to be more stable than free micelles or the micelles that are loaded with small molecule alone. This is supported by the data from Dox release study: Dox formulated in the co-loaded nanoparticles exhibited a slower kinetics of release compared to the formulation that is loaded with Dox only (Figure 3d). More studies will be conducted in the future to further address the stability of the co-loaded nanomicelles in vivo.

The complexes of DNA with POEG-*st*-Pmor polymer were significantly more stable than PEI/DNA complexes following exposure to BSA (30 mg/mL). This is likely due to the dynamic shielding of the complexes by PEG despite the fact that both complexes remain positively charged[50]. The improved stability of the complexes in the presence of serum proteins may contribute to the efficient delivery of DNA to distant s.c. tumors (Figure 6). A more effective accumulation in the lung is likely due to the interaction of tertiary amine moiety with negatively charged cell membrane in the lung[51, 52]. Amine-containing basic compounds have been reported to be predominantly accumulated in the lung due to the specific binding to acidic phospholipids on the cell membrane, which is abundantly distributed in lung tissue[53, 54]. Therefore our carriers are suitable for codelivery of nucleic acid therapeutics and small molecule drugs to both distant solid tumors and lung metastatic lesions.

POEG-*st*-Pmor was more effective than PEI in transfecting either lungs or distant s.c. tumor tissues *in vivo* (Figure 6). The higher *in vivo* transfection efficiency of POEG-*st*-Pmor polymer might be due to the enhanced stability of DNA/POEG-*st*-Pmor complexes in blood circulation due to the PEG shielding. It is also possible that POEG-*st*-Pmor form more stable

complexes with DNA compared to PEI. It has been reported that single or double-strand DNA could bind to nanoparticles through electrostatic, π-π stacking and hydrophobic interactions or even central cavity insertion[55–57]. In addition to charge-charge interaction, the hydrophobic backbone of our polymers and the pendant benzene rings can further interact with the base π-systems of nucleic acids through π-π stacking and hydrophobic interactions[58]. This was supported by the result from competitive binding gel-shift assay that the pDNA could hardly be released from POEG-*st*-Pmor micelles by dextran sulfate at an S/P ratio as high as 60 (Figure 2B). In contrast, substantial amounts of DNA were released from DNA/PEI complexes by dextran sulfate at an S/P ratio as low as 15/1 (Figure 2B).

POEG-*st*-Pmor alone was not active in the 4T1.2 lung metastasis model. Free Dox or delivery of IL-36γ alone via POEG-*st*-Pmor polymer showed a significant activity in inhibiting the lung metastasis. Combination of the two led to a further improvement in antitumor activity as shown by both smallest number of tumor nodules in the lung and the lowest weights of the tumor-bearing lungs (Figure 7B, D&E). DOX is known to induce immunogenic cell death of tumor cells and enhance the recruitment of T cells, which was consistent with our flow study (Figure 8A–C). On the other hand, IL-36γ is effective in promoting the function of T cells through enhancing the production of IFN-γ as shown in Figure 8D–G. The synergistic effect between DOX and IL-36γ (Figure 8D–G) likely plays an important role in the overall antitumor activity (Figure 7).

Interestingly, the T_{reg} cells were also increased following treatment with IL-36γ plasmid, alone or in combination with Dox (Figure 8J–K). This may be due to high amounts of IFN-γ accumulated locally, which may trigger the induction of Foxp3 expression in T cells[59]. Combination of IL-36γ plasmid/Dox codelivery with other therapies that can block the conversion of $CD4^+CD25^-$ T cells to $CD4^+$ T_{regs} may help to further enhance the outcome of treatment.

In summary, we developed and systematically evaluated the potential of POEG-*st*-Pmor nanocarrier for codelivery of Dox and IL36γ plasmid. Stable and nanosized micelles co-loaded with plasmid and Dox could be readily prepared and were highly effective in delivery to lungs as well as distant s.c. tumors. Significantly improved antitumor activity was demonstrated with codelivery of Dox and IL36γ plasmid in comparison with other control groups in a 4T1.2 lung metastasis model. POEG-*st*-Pmor may represent a simple and effective deliver system for an optimal chemo-gene combination therapy.

Supplementary Material

Refer to Web version on PubMed Central for supplementary material.

Acknowledgments

Funding: This work was supported in part by NIH grants R01CA174305, R01CA219399 and R01CA223788.

References

[1]. Chaffer CL, Weinberg RA. A perspective on cancer cell metastasis. Science. 2011;331:1559–64. [PubMed: 21436443]

[2]. Liotta LA, Steeg PS, Stetler-Stevenson WG. Cancer metastasis and angiogenesis: an imbalance of positive and negative regulation. Cell. 1991;64:327–36. [PubMed: 1703045]

[3]. Chambers AF, Groom AC, MacDonald IC. Metastasis: dissemination and growth of cancer cells in metastatic sites. Nature Reviews Cancer. 2002;2:563–72. [PubMed: 12154349]

[4]. Minn AJ, Gupta GP, Siegel PM, Bos PD, Shu W, Giri DD, et al. Genes that mediate breast cancer metastasis to lung. Nature. 2005;436:518–24. [PubMed: 16049480]

[5]. Leo F, Cagini L, Rocmans Pa, Cappello M, Van Geel AN, Maggi G, et al. Lung metastases from melanoma: when is surgical treatment warranted? British journal of cancer. 2000;83:569–72. [PubMed: 10944593]

[6]. Bacci G, Rocca M, Salone M, Balladelli A, Ferrari S, Palmerini E, et al. High grade osteosarcoma of the extremities with lung metastases at presentation: treatment with neoadjuvant chemotherapy and simultaneous resection of primary and metastatic lesions. Journal of surgical oncology. 2008;98:415–20. [PubMed: 18792969]

[7]. Andre F, Slimane K, Bachelot T, Dunant A, Namer M, Barrelier A, et al. Breast cancer with synchronous metastases: trends in survival during a 14-year period. Journal of Clinical Oncology. 2004;22:3302–8. [PubMed: 15310773]

[8]. Pashkevich MA, Sigal BM, Plevritis SK. Modeling the transition of lung cancer from early to advanced stage. Cancer Causes & Control. 2009;20:1559–69. [PubMed: 19629730]

[9]. Murphy EA, Majeti BK, Barnes LA, Makale M, Weis SM, Lutu-Fuga K, et al. Nanoparticle-mediated drug delivery to tumor vasculature suppresses metastasis. Proceedings of the National Academy of Sciences. 2008;105:9343–8.

[10]. Bisht S, Mizuma M, Feldmann G, Ottenhof NA, Hong S-M, Pramanik D, et al. Systemic administration of polymeric nanoparticle-encapsulated curcumin (NanoCurc) blocks tumor growth and metastases in preclinical models of pancreatic cancer. Molecular cancer therapeutics. 2010;9:2255–64. [PubMed: 20647339]

[11]. Couvreur P, Vauthier C. Nanotechnology: intelligent design to treat complex disease. Pharmaceutical research. 2006;23:1417–50. [PubMed: 16779701]

[12]. Maeda H, Wu J, Sawa T, Matsumura Y, Hori K. Tumor vascular permeability and the EPR effect in macromolecular therapeutics: a review. Journal of controlled release. 2000;65:271–84. [PubMed: 10699287]

[13]. Ackerman NB. The blood supply of experimental liver metastases. IV. Changes in vascularity with increasing tumor growth. Surgery. 1974;75:589–96. [PubMed: 4840805]

[14]. Hoet PHM, Nemery B. Polyamines in the lung: polyamine uptake and polyamine-linked pathological or toxicological conditions. American Journal of Physiology-Lung Cellular and Molecular Physiology. 2000;278:L417–L33. [PubMed: 10710513]

[15]. Zhou M, Li J, Li C, Guo L, Wang X, He Q, et al. Tertiary amine mediated targeted therapy against metastatic lung cancer. Journal of Controlled Release. 2016;241:81–93. [PubMed: 27639682]

[16]. Shi Y, van Steenbergen MJ, Teunissen EA, Novo Ls, Gradmann S, Baldus M, et al. Π–Π stacking increases the stability and loading capacity of thermosensitive polymeric micelles for chemotherapeutic drugs. Biomacromolecules. 2013;14:1826–37. [PubMed: 23607866]

[17]. Taton M, Benveniste P, Rahier A. Mechanism of inhibition of sterol biosynthesis enzymes by N-substituted morpholines. Pest Management Science. 1987;21:269–80.

[18]. Anderson MW, Orton TC, Pickett RD, Eling TE. Accumulation of amines in the isolated perfused rabbit lung. Journal of Pharmacology and Experimental Therapeutics. 1974;189:456–66. [PubMed: 4151395]

[19]. Yung BC, Li J, Zhang M, Cheng X, Li H, Yung EM, et al. Lipid nanoparticles composed of quaternary amine-tertiary amine cationic lipid combination (QTsome) for therapeutic delivery of AntimiR-21 for lung cancer. Molecular pharmaceutics. 2016;13:653–62. [PubMed: 26741162]

[20]. Gao Z-G, Tian L, Hu J, Park I-S, Bae YH. Prevention of metastasis in a 4T1 murine breast cancer model by doxorubicin carried by folate conjugated pH sensitive polymeric micelles. Journal of controlled release. 2011;152:84–9. [PubMed: 21295088]

[21]. Xiao J, Duan X, Yin Q, Zhang Z, Yu H, Li Y Nanodiamonds-mediated doxorubicin nuclear delivery to inhibit lung metastasis of breast cancer. Biomaterials. 2013;34:9648–56. [PubMed: 24016858]

[22]. Sampath P, Hanes J, DiMeco F, Tyler BM, Brat D, Pardoll DM, et al. Paracrine immunotherapy with interleukin-2 and local chemotherapy is synergistic in the treatment of experimental brain tumors. Cancer research. 1999;59:2107–14. [PubMed: 10232596]

[23]. Ramakrishnan R, Gabrilovich DI. Mechanism of synergistic effect of chemotherapy and immunotherapy of cancer. Cancer immunology, immunotherapy. 2011;60:419–23. [PubMed: 20976448]

[24]. Wang X, Zhao X, Feng C, Weinstein A, Xia R, Wen W, et al. IL-36y transforms the tumor microenvironment and promotes type 1 lymphocyte-mediated antitumor immune responses. Cancer cell. 2015;28:296–306. [PubMed: 26321222]

[25]. Carrier Y, Ma H-L, Ramon HE, Napierata L, Small C, O'Toole M, et al. Inter-regulation of Th17 cytokines and the IL-36 cytokines in vitro and in vivo: implications in psoriasis pathogenesis. Journal of Investigative Dermatology. 2011;131:2428–37. [PubMed: 21881584]

[26]. Lavasanifar A, Samuel J, Kwon GS. Micelles self-assembled from poly (ethylene oxide)-block-poly (N-hexyl stearate L-aspartamide) by a solvent evaporation method: effect on the solubilization and haemolytic activity of amphotericin B. Journal of Controlled Release. 2001;77:155–60. [PubMed: 11689268]

[27]. Sun J, Chen Y, Li K, Huang Y, Fu X, Zhang X, et al. A prodrug micellar carrier assembled from polymers with pendant farnesyl thiosalicylic acid moieties for improved delivery of paclitaxel. Acta Biomater. 2016;43:282–91. [PubMed: 27422196]

[28]. Chen Y, Xia R, Huang Y, Zhao W, Li J, Zhang X, et al. An immunostimulatory dual-functional nanocarrier that improves cancer immunochemotherapy. Nature Communications. 2016.

[29]. Chen Y, Zhang X, Lu J, Huang Y, Li J, Li S. Targeted delivery of curcumin to tumors via PEG-derivatized FTS-based micellar system. The AAPS journal. 2014;16:600–8. [PubMed: 24706375]

[30]. Zhang X, Huang Y, Zhao W, Liu H, Marquez R, Lu J, et al. Targeted Delivery of Anticancer Agents via a Dual Function Nanocarrier with an Interfacial Drug-Interactive Motif. Biomacromolecules. 2014;15:4326–35. [PubMed: 25325795]

[31]. Fischer D, Bieber T, Li Y, Elsasser H-P, Kissel T. A novel non-viral vector for DNA delivery based on low molecular weight, branched polyethylenimine: effect of molecular weight on transfection efficiency and cytotoxicity. Pharmaceutical research. 1999;16:1273–9. [PubMed: 10468031]

[32]. Gerlier D, Thomasset N. Use of MTT colorimetric assay to measure cell activation. Journal of immunological methods. 1986;94:57–63. [PubMed: 3782817]

[33]. Sun J, Liu Y, Chen Y, Zhao W, Zhai Q, Rathod S, et al. Doxorubicin delivered by a redox-responsive dasatinib-containing polymeric prodrug carrier for combination therapy. J Control Release. 2017;258:43–55. [PubMed: 28501705]

[34]. Venkataraman S, Ong WL, Ong ZY, Loo SCJ, Ee PLR, Yang YY. The role of PEG architecture and molecular weight in the gene transfection performance of PEGylated poly (dimethylaminoethyl methacrylate) based cationic polymers. Biomaterials. 2011;32:2369–78. [PubMed: 21186058]

[35]. Rungsardthong U, Deshpande M, Bailey L, Vamvakaki M, Armes SP, Garnett MC, et al. Copolymers of amine methacrylate with poly (ethylene glycol) as vectors for gene therapy. J Control Release. 2001;73:359–80. [PubMed: 11516512]

[36]. Sun J, Luo T, Sheng R, Li H, Chen S, Hu F, et al. Preparation of functional water-soluble low-cytotoxic poly(methacrylate)s with pendant cationic l-lysines for efficient gene delivery. Macromol Biosci. 2013;13:35–47. [PubMed: 23225764]

[37]. Whitehead KA, Langer R, Anderson DG. Knocking down barriers: advances in siRNA delivery. Nature reviews Drug discovery. 2009;8:129–38. [PubMed: 19180106]

[38]. Wagner V, Dullaart A, Bock A-K, Zweck A. The emerging nanomedicine landscape. Nature biotechnology. 2006;24:1211–7.

[39]. Bloomfield VA. Condensation of DNA by multivalent cations: considerations on mechanism. Biopolymers: Original Research on Biomolecules. 1991;31:1471–81.

[40]. Katayose S, Kataoka K. Water-soluble polyion complex associates of DNA and poly (ethylene glycol)- poly (l-lysine) block copolymer. Bioconjug Chem. 1997;8:702–7. [PubMed: 9327134]

[41]. Kim S, Shi Y, Kim JY, Park K, Cheng J-X. Overcoming the barriers in micellar drug delivery: loading efficiency, in vivo stability, and micelle-cell interaction. Expert opinion on drug delivery. 2010;7:49–62. [PubMed: 20017660]

[42]. Kataoka K, Harada A, Nagasaki Y. Block copolymer micelles for drug delivery: design, characterization and biological significance. Advanced drug delivery reviews. 2001;47:113–31. [PubMed: 11251249]

[43]. Lu J, Owen SC, Shoichet MS. Stability of self-assembled polymeric micelles in serum. Macromolecules. 2011;44:6002–8. [PubMed: 21818161]

[44]. Owen SC, Chan DPY, Shoichet MS. Polymeric micelle stability. Nano Today.2012;7:53–65.

[45]. Kwon GS, Yokoyama M, Okano T, Sakurai Y, Kataoka K. Biodistribution of micelle-forming polymer-drug conjugates. Pharmaceutical research. 1993;10:970–4. [PubMed: 8378259]

[46]. Miller T, Rachel R, Besheer A, Uezguen S, Weigandt M, Goepferich A. Comparative investigations on in vitro serum stability of polymeric micelle formulations. Pharmaceutical research. 2012;29:448–59. [PubMed: 21879388]

[47]. Rijcken CJ, Snel CJ, Schiffelers RM, van Nostrum CF, Hennink WE. Hydrolysable core-crosslinked thermosensitive polymeric micelles: synthesis, characterisation and in vivo studies. Biomaterials. 2007;28:5581–93. [PubMed: 17915312]

[48]. Dai J, Lin S, Cheng D, Zou S, Shuai X. Interlayer-Crosslinked Micelle with Partially Hydrated Core Showing Reduction and pH Dual Sensitivity for Pinpointed Intracellular Drug Release. Angewandte Chemie International Edition. 2011;50:9404–8. [PubMed: 21898731]

[49]. Talelli M, Iman M, Varkouhi AK, Rijcken CJF, Schiffelers RM, Etrych T, et al. Core-crosslinked polymeric micelles with controlled release of covalently entrapped doxorubicin. Biomaterials. 2010;31:7797–804. [PubMed: 20673684]

[50]. Fella C, Walker GF, Ogris M, Wagner E. Amine-reactive pyridylhydrazone-based PEG reagents for pH-reversible PEI polyplex shielding. european journal of pharmaceutical sciences. 2008;34:309–20. [PubMed: 18586470]

[51]. Pack DW, Hoffman AS, Pun S, Stayton PS. Design and development of polymers for gene delivery. Nature reviews Drug discovery. 2005;4:581–93. [PubMed: 16052241]

[52]. Patil ML, Zhang M, Minko T. Multifunctional triblock nanocarrier (PAMAM-PEG-PLL) for the efficient intracellular siRNA delivery and gene silencing. ACS nano. 2011;5:1877–87. [PubMed: 21322531]

[53]. Murakami T, Yumoto R. Role of phosphatidylserine binding in tissue distribution of amine-containing basic compounds. Expert opinion on drug metabolism & toxicology. 2011;7:353–64. [PubMed: 21332386]

[54]. Chander A, Johnson RG, Reicherter J, Fisher AB. Lung lamellar bodies maintain an acidic internal pH. Journal of Biological Chemistry. 1986;261:6126–31. [PubMed: 3700387]

[55]. Jeng ES, Barone PW, Nelson JD, Strano MS. Hybridization Kinetics and Thermodynamics of DNA Adsorbed to Individually Dispersed Single-Walled Carbon Nanotubes. Small. 2007;3:1602–9. [PubMed: 17786899]

[56]. Zheng M, Jagota A, Strano MS, Santos AP, Barone P, Chou SG, et al. Structure-based carbon nanotube sorting by sequence-dependent DNA assembly. Science. 2003;302:1545–8. [PubMed: 14645843]

[57]. Mu Q, Jiang G, Chen L, Zhou H, Fourches D, Tropsha A, et al. Chemical basis of interactions between engineered nanoparticles and biological systems. Chem Rev. 2014;114:7740–81. [PubMed: 24927254]

[58]. Matta CF, Castillo N, Boyd RJ. Extended weak bonding interactions in DNA: π-stacking (base-base), base- backbone, and backbone- backbone interactions. The Journal of Physical Chemistry B. 2006;110:563–78. [PubMed: 16471569]

[59]. Wang Z, Hong J, Sun W, Xu G, Li N, Chen X, et al. Role of IFN-y in induction of Foxp3 and conversion of CD4+ CD25-T cells to CD4+ Tregs. Journal of Clinical Investigation. 2006;116:2434. [PubMed: 16906223]

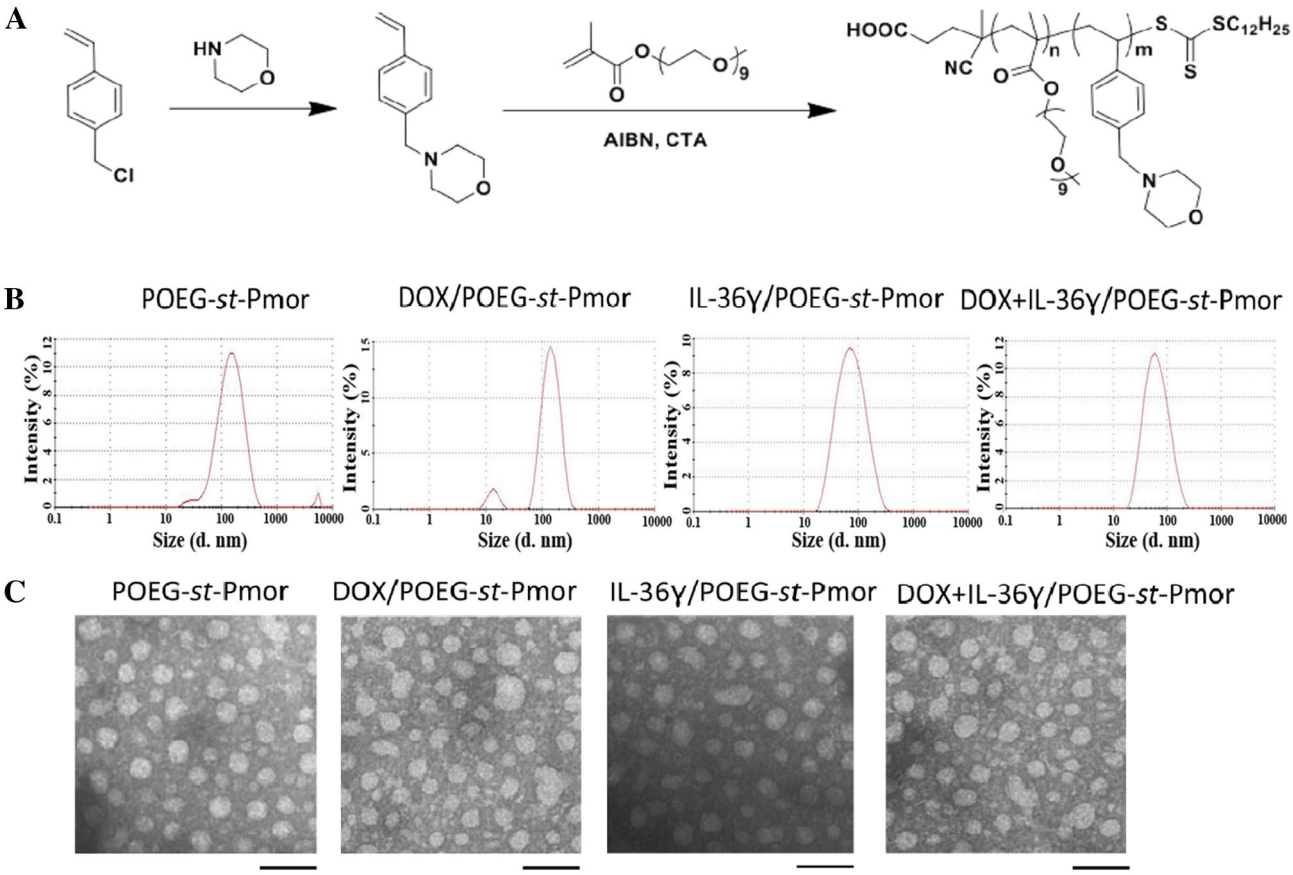

Figure 1.

(A) Synthesis scheme of POEG-*st*-Pmor polymer by RAFT co-polymerization of VBMor monomer and OEG500 monomer; (B) Particle size distribution and (C) TEM images of blank micelles, Dox-loaded micelles, IL-36γ plasmid complexed micelles and micelles co-loaded with IL-36γ plasmid and DOX. Scale bars: 100 nm.

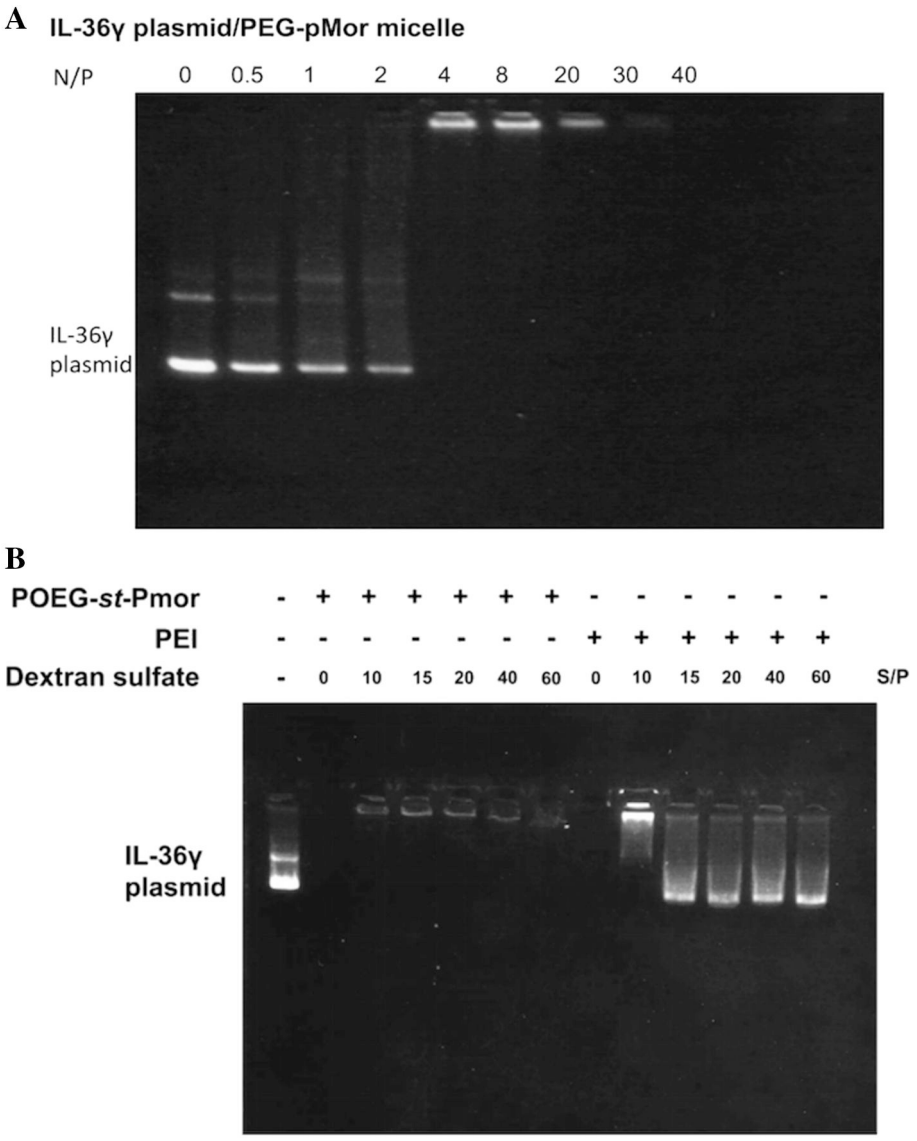

Figure 2.

Gel retardation assay of IL-36γ plasmid/polymer complexes at different N/P ratios. Samples were incubated for 20 min at room temperature before being loaded onto a 1% (w/v) agarose gel (100 V, 30 min). Representative gel images of plasmid/POEG-*st*-Pmor polymer (A) are shown from three independent experiments. (B) Dextran sulfate competitive binding gel electrophoresis assay for vector/plasmid complexes (N/P = 20) at various S/P ratios.

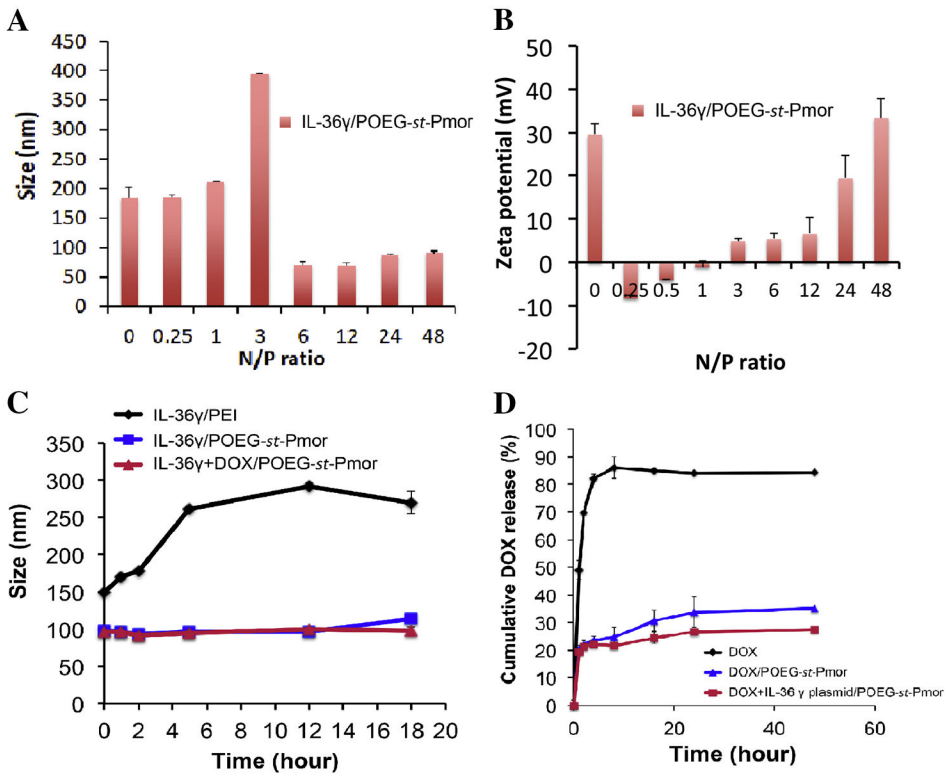

Figure 3.

Particle sizes (A) and zeta potentials (B) of IL-36γ plasmid/POEG-*st*-Pmor complexes formed at different N/P ratios. Data are expressed as means ± s.e.m. (n=3). (C) The stability of DOX+IL-36γ plasmid/POEG-*st*-Pmor was examined by incubating complexes (1 mg DOX/mL in PBS, pH 7.4) with bovine serum albumin (BSA, 30mg/mL) at 37°C. Changes in sizes of the complexes over incubation time were followed by DLS. (D) *In vitro* drug release profiles of DOX from free DOX, DOX/POEG-*st*-Pmor, and DOX+IL-36γ plasmid/POEG-*st*-Pmor in PBS at 37°C. Data are mean ± s.e.m. (n=3).

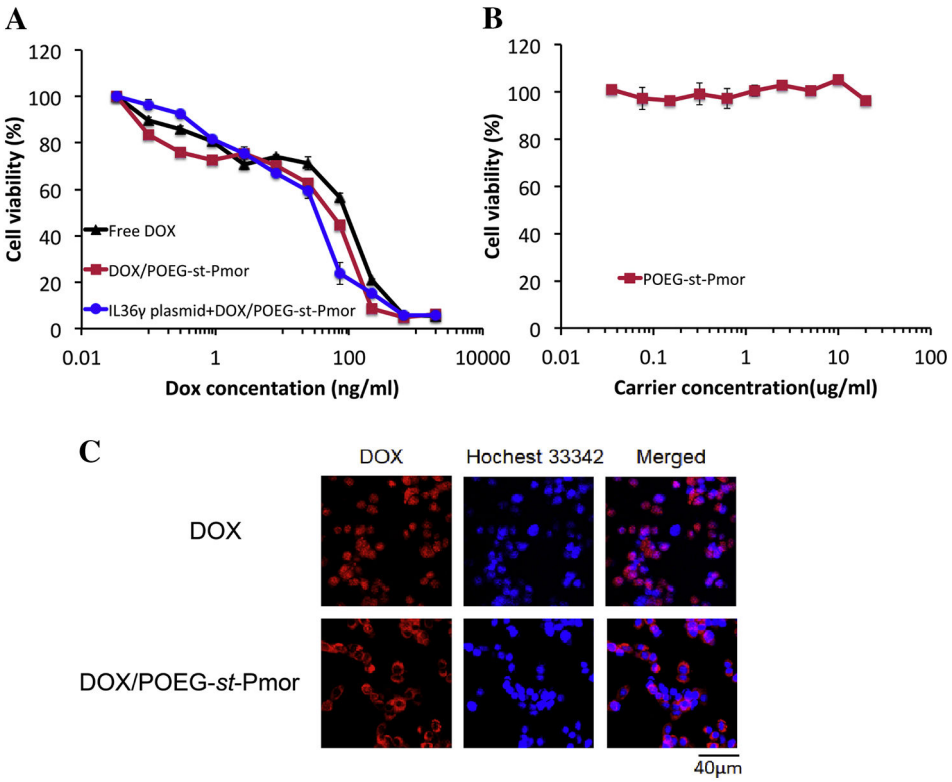

Figure 4.

(A) *In vitro* cytotoxicity of DOX+IL-36γ plasmid/POEG-*st*-Pmor in 4T1.2 cells. (B) *In vitro* cytotoxicity of drug-free micelles. Cells were treated for 72 h, and cytotoxicity was determined by MTT assay. Values were reported as means ± s.e.m. from triplicate samples. (C) Cellular uptake of free DOX and DOX-loaded POEG-*st*-Pmor micelles in 4T1.2 cancer cells at 2 h of incubation. Cell nuclei were stained with Hoechst 33342.

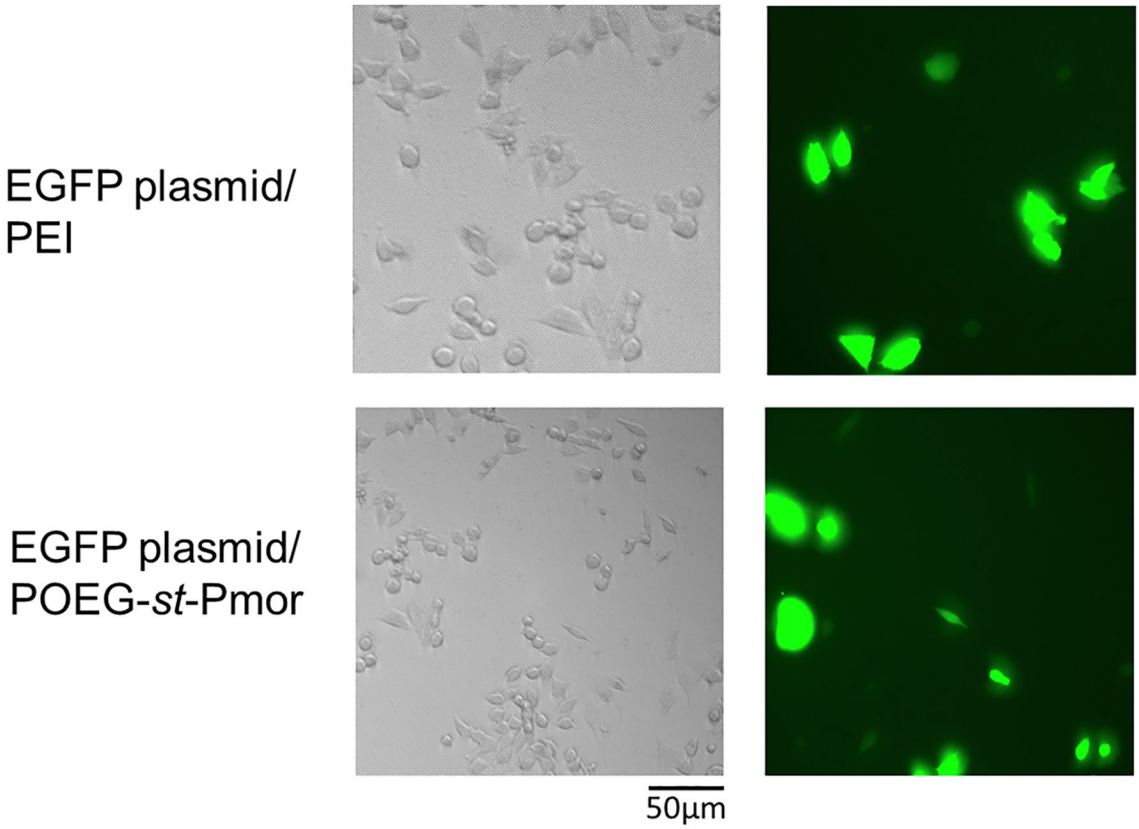

Figure 5.
Expression of EGFP 48 h following transfection of 4T1.2 cells with pEGFP-C1 plasmid complexed with PEI or POEG-*st*-Pmor.

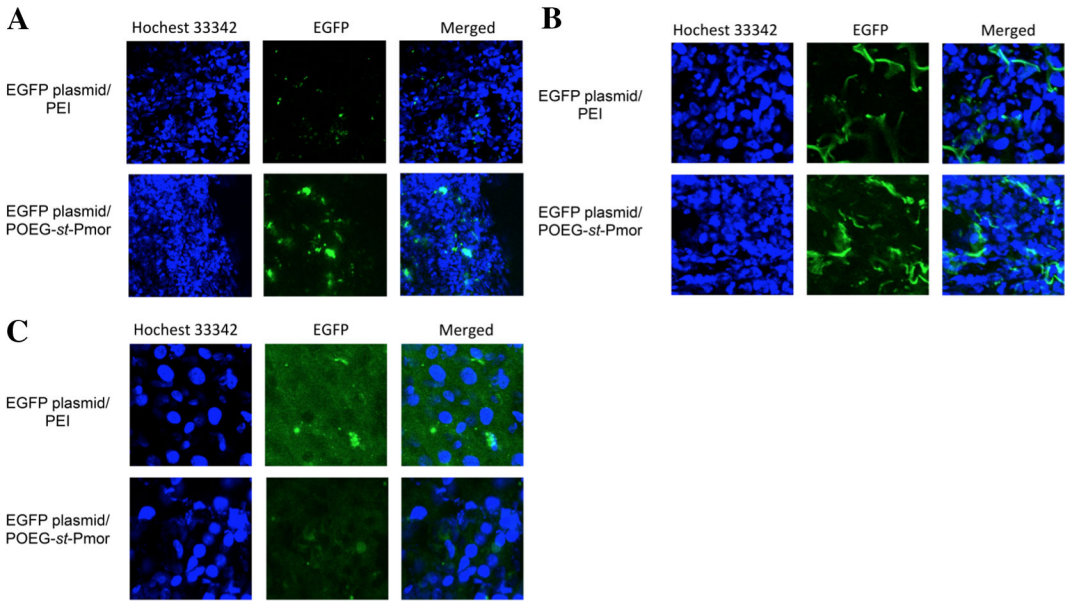

Figure 6.

In vivo EGFP expression in liver, lung and tumor tissues. Balb/c mice bearing 4T1.2 tumor were i.v. injected with EGFP plasmid/PEI and EGFP plasmid/POEG-*st*-Pmor. EGFP expression in (A) tumor, (B) lung, and (C) liver was examined 24 h later.

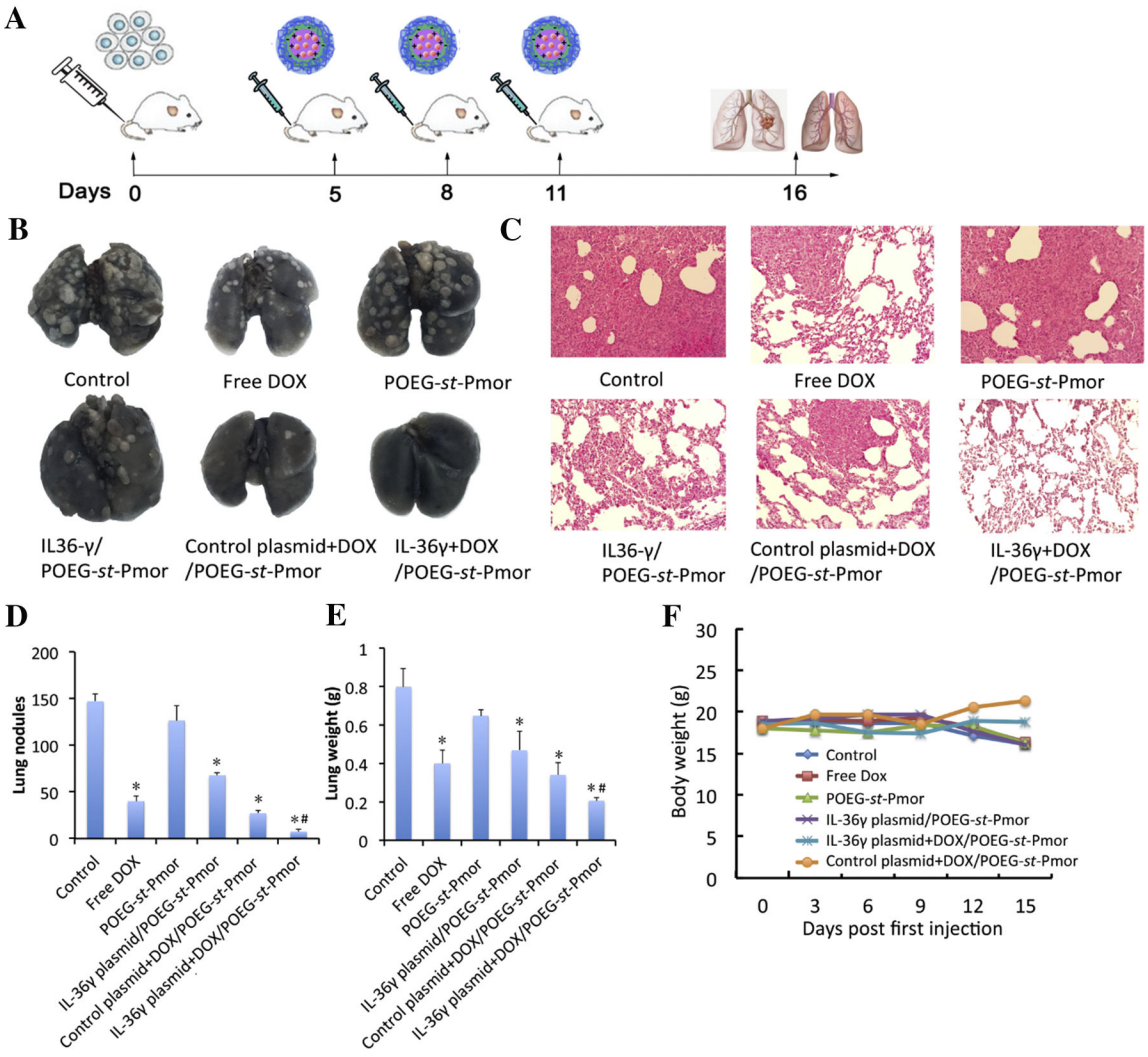

Figure 7.

Synergistic antitumor activity of IL36γ plasmid and DOX codelivered by POEG-*st*-Pmor micelles in a mouse model of breast cancer (4T1.2) lung metastasis. (A) experimental scheme for the establishment of lung metastasis and treatment. (B) representative gross images of lungs collected from mice receiving various treatments. (C) H&E staining of lung tissues. (D) Quantification of tumor nodules. (E) Mouse lung weights (n = 5). (F) Changes in mouse body weights during the treatment period. Data are presented as the means ± SEM. *$p < 0.05$ versus control.

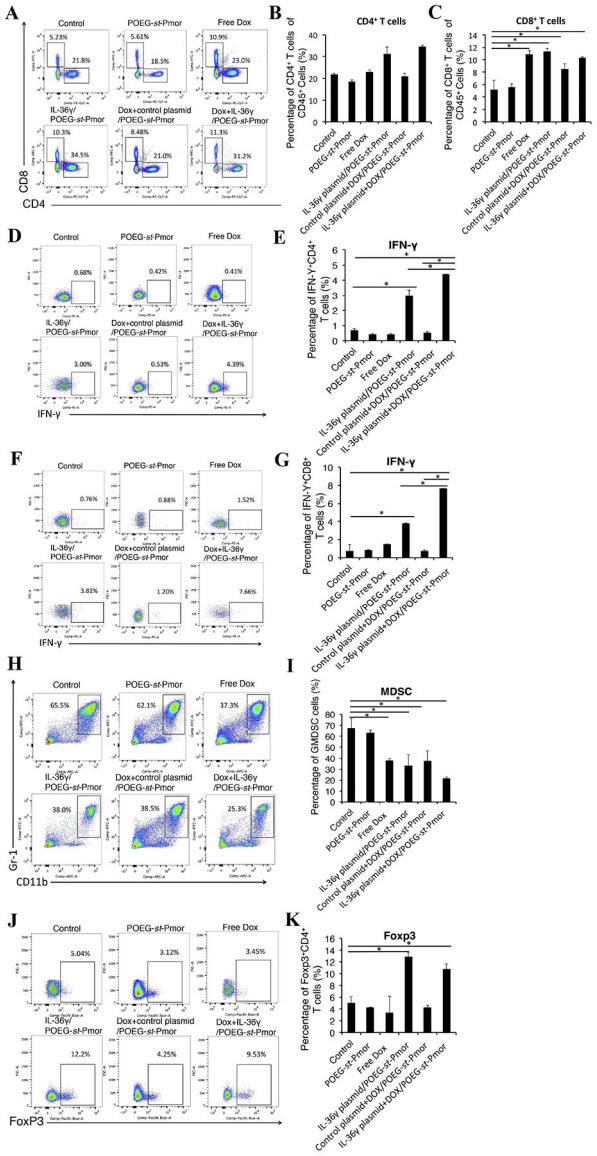

Figure 8.

Flow analysis of infiltration of immune cells in tumor-bearing lungs following various treatments. Balb/c mice were injected with 2×10^5 4T1.2 cells via tail vein. Five days later, mice were treated with POEG-*st*-Pmor carrier, free Dox, IL-36γplasmid/POEG-*st*-Pmor, Dox+control plasmid/POEG-*st*-Pmor and Dox+IL-36γplasmid/POEG-*st*-Pmor, respectively for three times. (A-C) T lymphocyte subsets isolated from lung tissues with 4T1.2 metastasis were analyzed by flow cytometry. The percentage of $CD4^+$ and $CD8^+$ T cells in the lung tissues with various treatments was determined by flow cytometry analysis. (D-G) IL-36γ plasmid/micelles increased the $IFN\gamma^+$ $CD4^+$ and $IFN\gamma^+$ $CD8^+$ T cells in tumor-bearing lungs. (H-I) MDSCs were stained with CD11b and Gr-1 antibody and determined by flow cytometry. (J-K) flow analysis of $Foxp3^+$ T regulatory cells in mouse lungs. The results are shown as the means ± SEM of 3 mice in each group. *$P<0.05$.

Table 1.

Biophysical characteristics of blank micelles and the micelles co-loaded with IL-36γ plasmid and DOX

Micelles	Mass ratio (mg: mg)	N/P ratio	Size (nm)	Zeta potential (mV)	Stability
POEG-*st*-Pmor	--	--	184±3.5	26.4±1.1	--
IL-36γ/POEG-*st*-Pmor	--	20	95.0±1.8	10.3 ± 0.1	--
	10:1	--	178 ± 2.1	27.1 ±0.7	2 weeks
DOX/POEG-*st*-Pmor	20:1	--	174±1.5	24.7 ± 0.9	4 weeks
	30:1	--	162±4.1	26.0 ± 0.7	1 month
DOX+IL-36γ/POEG-*st*-Pmor	20:1	20	84.4±1.7	10.4 ± 0.2	1 month

*The colloidal stability was followed at room temperature by measuring the size and observing precipitates.